NANO LETTERS
Letter
Cite This: Nano Lett. 2018, 18, 2630−2636
pubs.acs.org/NanoLett

Light-Responsive Polymer Particles as Force Clamps for the Mechanical Unfolding of Target Molecules

Hanquan Su,[†] Zheng Liu,[†,§] Yang Liu,[†,∥] Victor Pui-Yan Ma,[†] Aaron Blanchard,[‡] Jing Zhao,[†] Kornelia Galior,[†] R. Brian Dyer,[†] and Khalid Salaita*[,†,‡]

[†]Department of Chemistry, Emory University, Atlanta, Georgia 30322, United States
[‡]Wallace H. Coulter Department of Biomedical Engineering, Georgia Institute of Technology and Emory University, Atlanta, Georgia 30322, United States

Supporting Information

ABSTRACT: Single-molecule force spectroscopy techniques are powerful tools for investigating the mechanical unfolding of biomolecules. However, they are limited in throughput and require dedicated instrumentation. Here, we report a force-generating particle that can unfold target molecules on-demand. The particle consists of a plasmonic nanorod core encapsulated with a thermoresponsive polymer shell. Optical heating of the nanorod leads to rapid collapse of the polymer, thus transducing light into mechanical work to unfold target molecules. The illumination tunes the duration and degree of particle collapse, thus controlling the lifetime and magnitude of applied forces. Single-molecule fluorescence imaging showed reproducible mechanical unfolding of DNA hairpins. We also demonstrate the triggering of 50 different particles in <1 min, exceeding the speed of conventional atomic force microscopy. The polymer force clamp represents a facile and bottom-up approach to force manipulation.

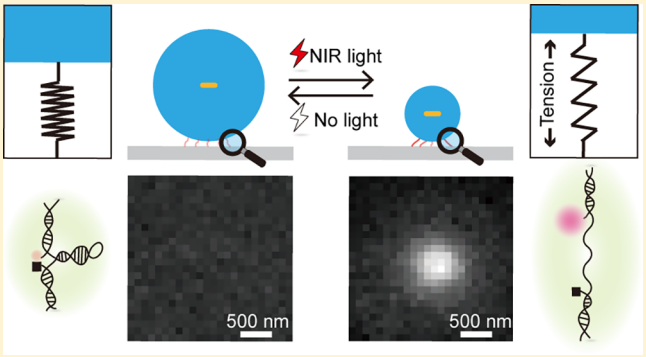

KEYWORDS: *Core−shell particle, responsive materials, force spectroscopy, gold nanoparticles, DNA unfolding*

Tools such as atomic force microscopy (AFM)[1−4] along with optical[5−7] and magnetic[8] tweezers have opened the door to studying the mechanical unfolding of biomolecules. However, these techniques are low-throughput, require dedicated and complex instrumentation,[9] and also require linking the target molecule of interest to the force probe.[10] One approach to increasing the throughput is centrifuge force microscopy (CFM), with which Wong and co-workers retrofitted a standard centrifuge to spin a sample containing microbeads anchored through a molecule of interest.[11,12] More recently, Liedl and colleagues showed that bracket-shaped DNA origami structures can clamp target DNA molecules at a defined extension.[13] This was a noteworthy development and, in contrast to CFM, avoids the need for instrumentation because the force-generating unit is synthesized bottom-up. Nonetheless, each origami clamp is fixed and does not allow for dynamic modulation of the applied force. This is an important capability as recent evidence shows that the rate of folding (and unfolding), and the force responses are highly dependent on the dynamic history of a bond.[14,15] Therefore, it is important to develop methods of dynamically applying forces using force-generating nanomaterials.

Herein, we report a polymer force clamp (PFC), which can deliver pN forces to target biomolecules of interest leading to controlled unfolding. The general design of the PFC is illustrated in Scheme 1 and is based on our recently published work, in which these polymer particles were used to trigger receptor activation in living cells.[16] This past work suggested that multiple layers of these particles can be cross-linked to DNA with biotin−streptavidin to apply pN scale forces, which led us to the current investigations. The PFC is

Scheme 1. Schematic Comparing Force Spectroscopy Using a Conventional Atomic Force Microscope and Our Polymer Force Clamp

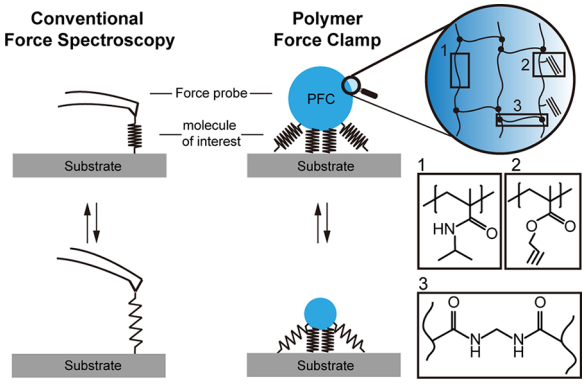

Received: February 1, 2018
Revised: February 22, 2018
Published: March 28, 2018

DOI: 10.1021/acs.nanolett.8b00459
Nano Lett. 2018, 18, 2630−2636

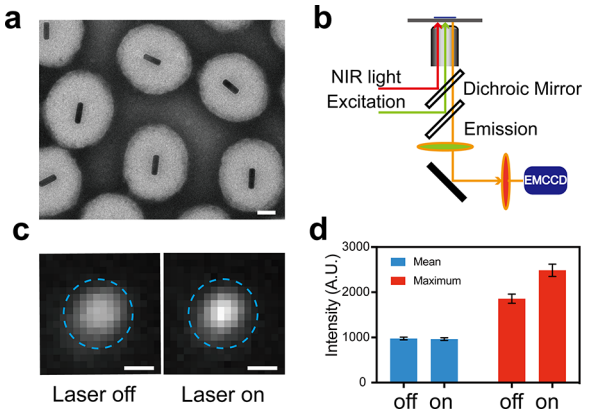

Figure 1. General design of the polymer force clamp (PFC). (a) Representative TEM image of PFC particles. Scale bar: 100 nm. (b) Optical configuration for simultaneous NIR illumination and fluorescence imaging. (c) Representative fluorescein images of labeled PFC particle irradiated with a 785 nm NIR laser beam at a power density of 0.75 mW/μm^2. Fluorescence within the blue circles was measured. Scale bar: 500 nm. (d) Plot displaying the mean and maximum intensity of PFC before and after NIR illumination. Error bars represent the standard deviation, n = 5.

composed of a gold nanorod core (~25 nm × 100 nm) as a photothermal transducer[17] coated with a 250 nm thermoresponsive poly-*N*-isopropylmethacrylamide (pNIPMAm) shell (Figures 1a and S1). We synthesized PFCs with a 250 nm polymer shell because modeling suggested that thermal energy is dissipated at a radius of 250 nm from the nanorod core (Figure S2). Therefore, near-infrared (NIR) illumination of the PFC leads to its collapse (from 550 to 310 nm based on the DLS, shown in Figure S3) generating an inward force applied to target biomolecules that are immobilized on a surface. To provide a convenient and modular handle for the attachment of target molecules, the PFC surface was decorated with alkyne groups amenable for Cu (I) catalyzed cycloaddition to any azide-modified target. The PFC particles were also labeled with fluorescein to validate the collapse of the particle following NIR triggering. Although any NIR source can be used to control the collapse of the PFC, we employed a commercially available galvo illuminator (Rapp Optoelectric, Germany) (Figure 1b) because this generated a 5 μm NIR spot controllable with μs time resolution (Figure S4).

Upon triggering by NIR, we observed an increase in the peak fluorescence intensity at the center of the fluorescein labeled PFC while the integrated intensity remained constant, thus showing optically triggered particle collapse (Figure 1c,d). Time-lapse imaging and line-scan analysis further confirm NIR-driven particle collapse (Figure S5 and Movie S1). These results show that we can perform simultaneous particle triggering and fluorescence imaging with high resolution.

We next investigated whether the PFC can mechanically clamp biomolecules. We focused our efforts on DNA hairpins because of their well-characterized digital force-response profiles and tunable mechanical properties[18]. The $F_{1/2}$ is defined as the equilibrium force that leads to a 50% probability of hairpin unfolding and can be easily tuned by changing the GC content of a hairpin stem.[19] In this study, we used two types of DNA hairpins with calibrated $F_{1/2}$ values of 4.7 and 13.1 pN (22% and 100% GC content stem, respectively).[20,21] To detect unfolding, we hybridized the hairpin with ligand strands and anchor strands that were functionalized with a fluorophore (Cy3B) and quencher (BHQ2), respectively, that undergo contact quenching (Figure 2a and Table S1). DNA hairpins were immobilized onto a glass coverslip that was decorated with 13 nm gold particles, providing an additional quenching mechanism.[22,23] The surface-anchored 4.7 pN DNA hairpin was coupled to the PFC using the click cycloaddition reaction (Figure S6). PFC surface density was reduced to facilitate the control and characterization of DNA unfolding by individual particles. When the particle was illuminated at a 1 Hz frequency and 50% duty cycle (500 ms illumination followed by 500 ms rest), we observed a rapid and concurrent increase in the fluorescein and Cy3B signal intensities (Figure 2b). Both channels reversibly responded to the NIR input and were spatially co-localized (Movie S2 and S3). We attributed the change in fluorescein signal to the physical collapse of the PFC, while the enhancement of Cy3B signal is due to the mechanical unfolding of the 4.7 pN DNA hairpin. 50 different PFCs were randomly selected across a single substrate whose size changes were first confirmed by imaging in the fluorescein channel. Then, the change in Cy3B intensity (ΔI) of each particle was measured (Supplementary Method) and plotted in a histogram (Figure 2b). The mean ΔI was 1145 ± 490 au, which corresponds to unfolding of 7.6 ± 3.8% of DNA hairpins under each particle (Figure S7 and S8). Given the DNA density as measured by AFM analysis (Figure S9) and bulk fluorescence measurements (Figure S10); this indicates that ~21 DNA hairpins ($F_{1/2}$ = 4.7 pN) were mechanically unfolded within the brightest pixel area (160 nm × 160 nm). Triggering different particles can be automated for rapid clamping measurements. Indeed, Figure S11 and Movie S4 show the triggering of 49 PFCs and measuring associated DNA unfolding in less than 1 min, which exceeds the throughput of a typical AFM clamping measurements by orders of magnitude.

Controls using non-extendable duplex DNA structure (Figure 2c) or covalently linking the particles to the glass instead of the DNA hairpin (Figures 2d and S12) confirmed that the Cy3B signal is due to mechanical unfolding of the DNA hairpin. In these controls, the fluorescein signal responded similarly to the experiments shown in Figure 2b (Movies S5 and S6), but the ΔI was 209 ± 36 au (Figure 2c) and 92 ± 68 au (Figure 2d and Movies S7 and S8). The weak Cy3B signals observed here are likely due to a combination of structural changes in the nicked DNA duplex following application of mechanical strain[6,24−26] as well as weak bleedthrough from the 785 nm NIR illumination (Figure S13). Furthermore, finite element analysis (Figure S14 and S15) predicts that the local temperature increase is insufficient to thermally denature the hairpin based on the melting curves for the DNA hairpins (T_m = 54 and 70 °C for the 22% and 100% GC content stems; Figure S16). Taken together, the experiments and theoretical stimulations confirm that the PFC mechanically clamps and unfolds target molecules. Therefore, to the best of our knowledge, this represents the first example of a force-generating polymer particle that can be triggered to unfold target molecules on demand.

Next, we compared the unfolding of the $F_{1/2}$ = 4.7 pN and 13.1 pN DNA hairpins (Figure 3a). Line-scan analysis confirmed that PFC particles on both surfaces showed collapse upon NIR stimulation. However, the tension signal (ΔI) for the 13.1 pN probes was significantly lower than that of the 4.7 pN probes (Figure 3b). A histogram plot of the ΔI for n = 50 particles on two different samples with similar DNA density (for each type of DNA probe) is shown in Figure 3c. The ΔI for the population of PFC particles shifted from a mean of

DOI: 10.1021/acs.nanolett.8b00459
Nano Lett. 2018, 18, 2630−2636

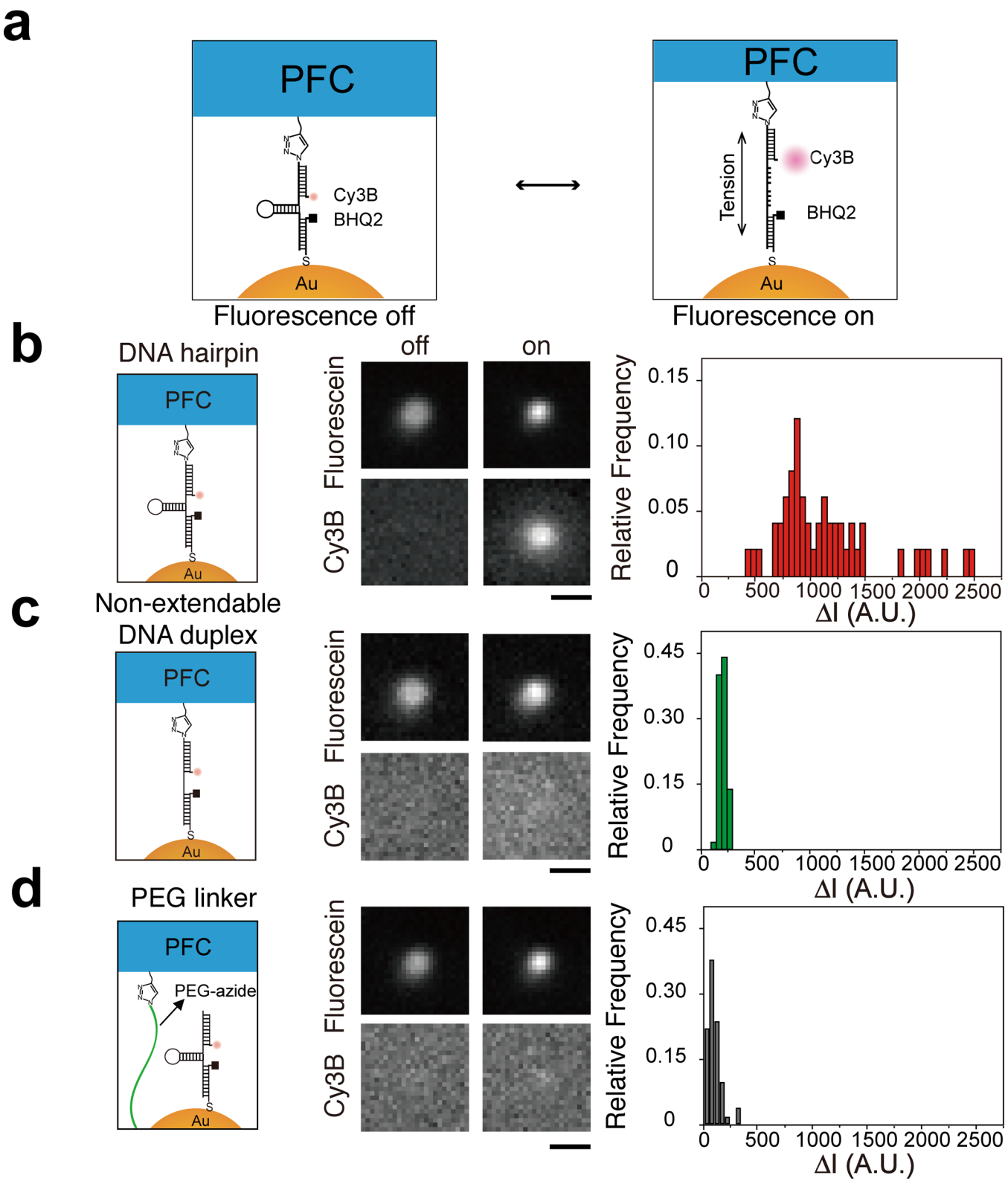

Figure 2. Mechanical clamping of DNA hairpins. (a) Schematic diagram. (b–d) Representative fluorescein/Cy3B images and histogram of change in Cy3B intensity from 50 individual PFCs tethered to (b) DNA hairpins, (c) non-extendable DNA duplexes, and (d) PEG linker. Scale bar: 1 μm. NIR power density: 0.75 mW/μm^2.

1145 ± 487 to 702 ± 498 au when the probe $F_{1/2}$ was increased from 4.7 to 13.1 pN. Given that we used identical DNA surface densities in these samples and the unfolding was performed using the same batch of PFC particles, the difference in ΔI is due to the innate difference in the free energy of unfolding the 4.7 and 13.1 pN hairpins. This suggests that more-stable DNA hairpins require greater mechanical work to drive unfolding, and thus, there are fewer unfolding events in the 13.1 pN sample. In other words, the experiment indicates that the PFC generates a limited amount of mechanical work that sets the

DOI: 10.1021/acs.nanolett.8b00459
Nano Lett. 2018, 18, 2630–2636

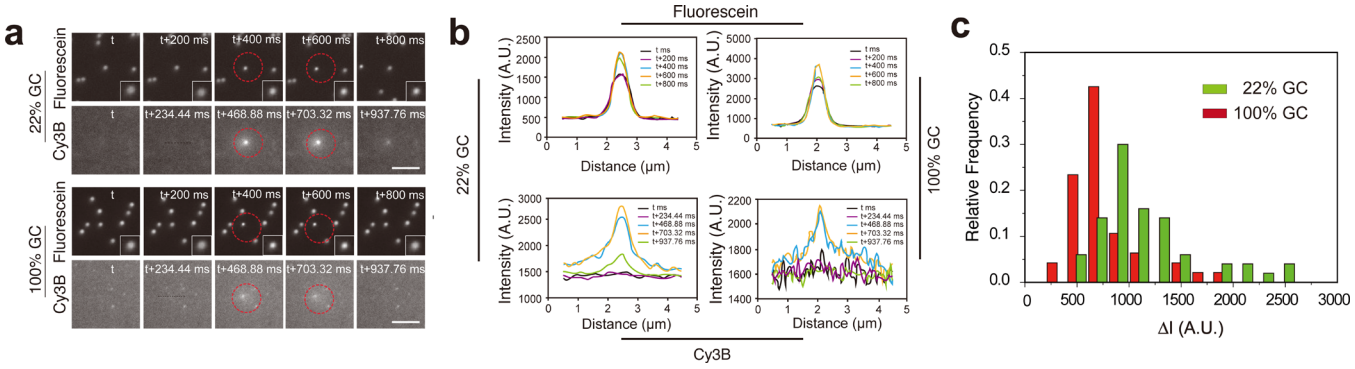

Figure 3. GC content influences unfolding. (a) Representative time-lapse fluorescein/Cy3B images of clamping the DNA hairpin with 22% and 100% GC content in a single illumination cycle (red circle, power density of 0.75 mW/μm^2, 1 Hz, 50% duty cycle). Scale bar: 5 μm. (b) Line-scan analysis plot of force-clamp and DNA hairpin fluorescence in one unfolding cycle. (c) Histogram of Cy3B ΔI values (unfolding) of 22% GC and 100% GC hairpin targets; n = 50.

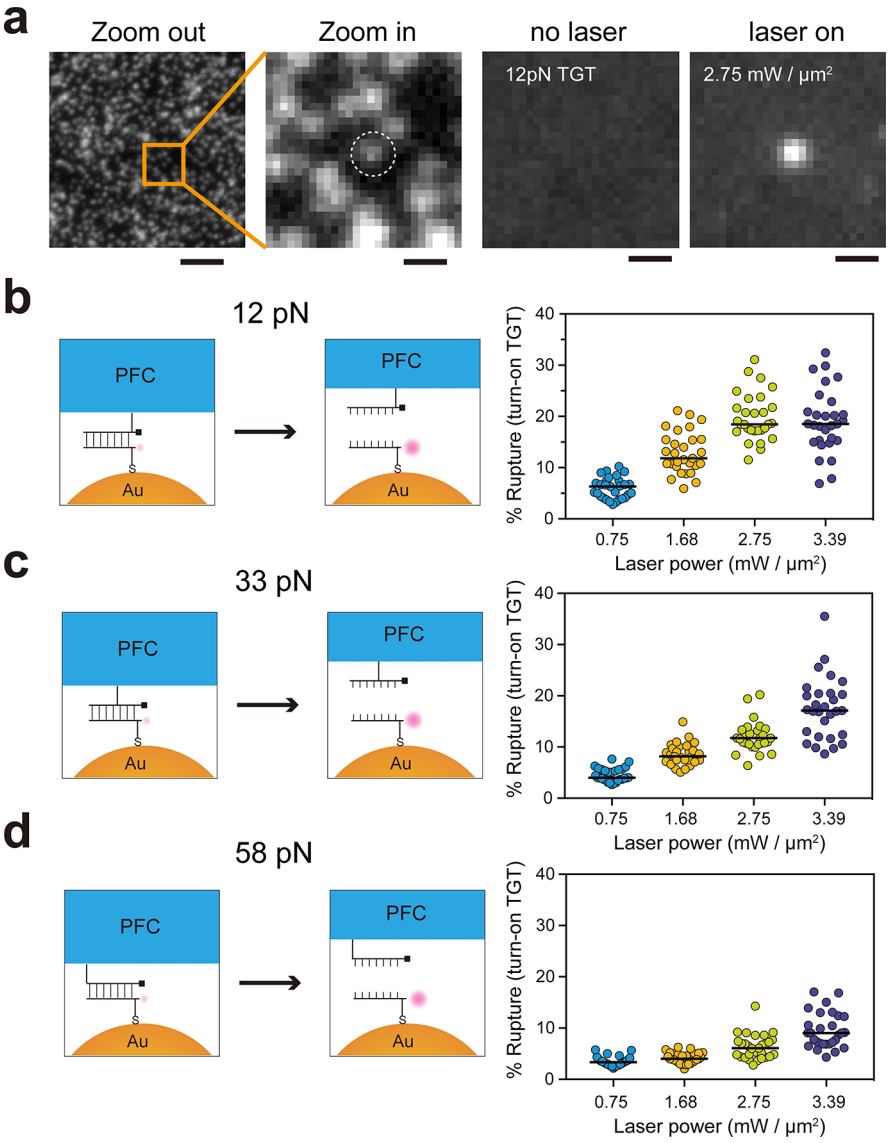

Figure 4. Mechanical unfolding of TGT. (a) The first two fluorescence images show fluorescein-labeled PFC particles immobilized onto a 12 pN TGT surface at two magnifications. The third and fourth images show the Cy3B 12 pN TGT signal before and after NIR illumination, respectively.. NIR power density = 2.75 mW/μm^2. Scale bar = 1 μm, except for first image, which is 5 μm. (b–d) Schematic and plots showing the fraction of ruptured TGTs as a function of laser power. TGT with T_{tol} = 12, 33, and 58 pN were tested.

total number of unfolded molecules during a collapse cycle with a given illumination profile (time and intensity).

To better define the force generated by each PFC as a function of laser power, we used the PFC to unfold DNA

DOI: 10.1021/acs.nanolett.8b00459
Nano Lett. 2018, 18, 2630–2636

duplexes that are described as tension gauge tethers (TGTs), which denature at a threshold value of force, tension tolerance (T_{tol}).[27−30] The T_{tol} is defined as the amount of force that leads to unfolding of a duplex within 2 s. If the PFC applies a force above T_{tol}, the tether will rupture and dequench the fluorophore (Figure 4a). The fraction of ruptured TGTs was calculated based on the fluorescence signal (Figures S17 and S18). We synthesized different TGT surfaces with T_{tol} = 12, 33, and 58 pN by positioning the anchor of the upper strand. A 2 s illumination at different laser powers was applied. Increasing the laser power leads to a general increase in the TGT signal. However, we found that the fraction of ruptured TGTs reached a plateau with the 2.75 mW/μm^2 laser power on the 12 pN TGT surface (Figure 4b), whereas a linear increase was observed on 33 pN TGT surface (Figure 4c). There was minimal TGT rupture of the T_{tol} = 58 pN probes (Figure 4d). These results define the range of applied forces using the calibrated TGT probes and thus demonstrate that the average force experienced per molecule can be tuned and enhanced up to ∼58 pN when employing the maximum illumination intensity of 3.39 mW/μm^2.

To demonstrate single-molecule unfolding with our force-generating particles, we reduced the labeling ratio of DNA to 1:10000. This dye-labeling ratio resulted in a small fraction (∼5%) of PFC particles that displayed single-molecule fluorescence. Single-molecule intensity was validated using control samples that were dequenched by hybridization and also by measuring single-step photobleaching (Figure S19). To mechanically unfold single labeled DNA hairpins, we used a power density of 0.75 mW/μm^2 (matching the conditions used in Figures 2 and 3) with an on-time of 450 ms followed by a 450 ms rest time. Figure 5a shows representative time-lapse imaging of a single hairpin reversibly unfolding due to PFC-generated forces. The EMCCD camera acquisition (16.67 frame/sec) was synchronized with the NIR illumination pulse sequence to average the force-induced unfolding traces from different PFC particles. Figure 5b shows the average fluorescence intensity from a 5 × 5 pixel region of interest during a 17 s NIR illumination sequence. Unfolding was characterized as a ∼450 au jump in fluorescence above the signal due to NIR background and could be measured for tens of cycles until the dye photobleached. A histogram of n = 900 single hairpin unfolding events from four different PFC particles exhibited a bimodal distribution of fluorescence intensity (Figure 5c). This distribution corresponds to the intensity of the folded and unfolded states of single DNA hairpins. Taken together, these experiments demonstrate that the PFC provides the ability to simultaneously manipulate and characterize the mechanical unfolding of individual target molecules.

Note that the PFC approach to unfolding carries several caveats. First, the applied force likely varies across the particle-surface junction. Molecules at the center of the junction likely experience weaker forces compared to the edges. Second, we observed particle−particle variability in DNA unfolding (Figure S20), which is due to the alignment of the linearly polarized source with the orientation of the nanorods (Figure S21).[31,32] Another source of variability is due to the monodispersity of the polymer shell and the gold nanorod, which is akin to tip-to-tip variability in AFM or bead-to-bead variability in optical and magnetic tweezer experiments. Nonetheless, when we probed 49 PFCs attached to the 13.1 pN DNA hairpin probe for two cycles, the individual particle response was generally reproducible (19% difference between the first and second cycles) (Figure S11 and Movie S4).

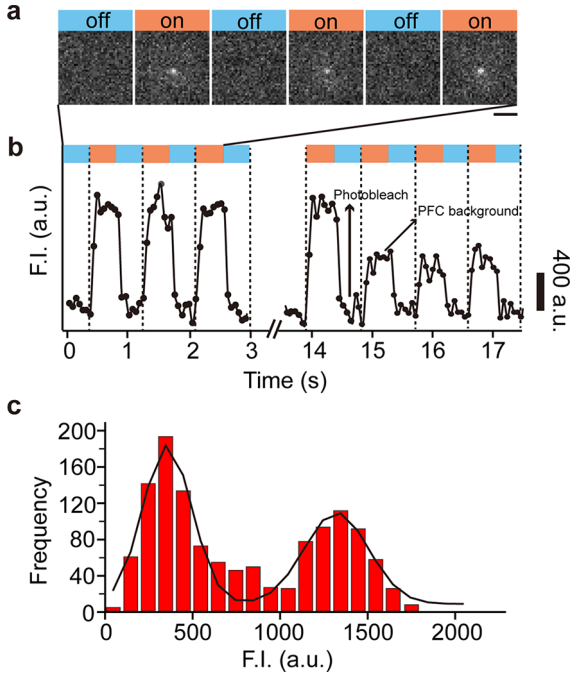

Figure 5. Monitoring the mechanical unfolding of a single DNA hairpin. (a) Representative time-lapse images of PFC-driven single hairpin unfolding. Scale bar: 2 μm. (b) Plot of the fluorescence intensity from data shown in panel a as a function of time (NIR stimulation). The signal during NIR illumination abruptly decreases at t = 15 s, which likely corresponds to photobleaching. The remaining signal during NIR illumination is due to background. The fluorescence intensity was calculated from a region of interest of 5 × 5 pixels. (c) Frequency histogram plotting the fluorescence intensity for 900 NIR illumination cycles collected from four different PFC particles. The signal was analyzed prior to photobleaching events.

In summary, our work demonstrates a novel approach for mechanically manipulating and unfolding target molecules. Forces are generated due to the volume phase transition of the polymer particle, and although in this report we focused on using light to trigger this process, it is possible to drive the volume phase transition using other stimuli such as pH, ionic strength, and temperature. Fundamentally, PFCs represent a bottom-up approach to force manipulation, in which each particle is a force generating unit akin to an AFM force probe. Therefore, massive parallelization of mechanical unfolding is, in principle, possible using an ensemble of PFCs. This is in contrast to conventional AFM and optical and magnetic tweezers, with which parallelization still represents a challenge.[9] Finally, time-resolved measurements of the volume phase transition of NIPAM nanogel particles indicate that the particle collapse occurs at the nanosecond time scale,[33,34] and thus, PFCs can potentially offer force manipulation at the nanoscale time scale, which is currently inaccessible to conventional methods.

■ ASSOCIATED CONTENT

Supporting Information

The Supporting Information is available free of charge on the ACS Publications website at DOI: 10.1021/acs.nanolett.8b00459.

Time-lapse RICM movie showing 100 cycles of PFC NIR illumination and collapse. (AVI)

Time-lapse fluorescence movie showing fluorescein-labeled PFC particles responding to NIR illumination on the 4.7 pN DNA hairpin surface. (AVI)

DOI: 10.1021/acs.nanolett.8b00459
Nano Lett. 2018, 18, 2630−2636

Time-lapse fluorescence movie showing change in fluorescence intensity due to the reversible mechanical unfolding of 4.7 pN DNA hairpin. (AVI)
Time-lapse fluorescence movie showing rapid screening of DNA hairpin unfolding by an array of PFCs. (AVI)
Time-lapse fluorescence movie showing fluorescein-labeled PFC collapse on the non-extendable DNA surface. (AVI)
Time-lapse fluorescence movie showing the collapse of PEG covalently linked PFCs. (AVI)
Time-lapse fluorescence movie showing the response of non-extendable DNA duplex upon PFC collapse. (AVI)
Time-lapse fluorescence movie showing the response of DNA hairpins upon PFC collapse when particles were anchored using PEG. (AVI)
Additional details on experimental materials and methods. Movie descriptions. A table showing oligonucleotide ID and sequences. Figures showing TEM images, heat distribution in a PFC particle, temperature-dependent DLS measurement, NIR illumination spot, volume phase transition of PFC, coupling of PFC to the DNA hairpin surface, determination of quenching efficiency of DNA hairpin, determination of DNA hairpin unfolding fraction, atomic force microscopy image of AuNPs, the process of determining stoichiometry between Cy3B-DNA hairpin and AuNP, integrated Cy3B signal intensity of 49 PFCs, minimal bleedthrough of NIR into Cy3B channel, finite element analysis simulation of extreme scenarios, melting curves of DNA hairpins, determination of TGT rupture fraction, a schematic showing single DNA hairpin unfolding, photobleaching of single Cy3B tagged DNA hairpin, particle−particle variability in DNA unfolding, illustration of the orientation of nanorods, optical-thermal energy conversion, and radian dependence of heat conversion (PDF)

AUTHOR INFORMATION

Corresponding Author

*E-mail: k.salaita@emory.edu. Phone: 404-727-7522.

ORCID

Jing Zhao: 0000-0003-1874-6524
R. Brian Dyer: 0000-0002-0090-7580
Khalid Salaita: 0000-0003-4138-3477

Present Addresses

[§]The Institute for Advanced Studies, Wuhan University, Wuhan, PR China.
[‖]Department of Biophysics and Biophysical Chemistry, Johns Hopkins University, Baltimore, MD, United States.

Author Contributions

H.S. and Z.L. contributed equally to this work. All authors have given approval to the final version of the manuscript. H.S., Z.L., B.D. and K.S. conceived and designed the experiments. H.S. and Z.L designed and assembled the PFC laser illumination system. H.S. and Z.L. performed the DNA unfolding experiments. H.S., Y.L. and K.G performed the surface modification. H.S. and V.M. performed the DNA modification. A.B carried out the MATLAB analysis. J.Z. carried out the COMSOL simulation. The manuscript was prepared by H.S. and K.S. with input from all authors.

Notes

The authors declare no competing financial interest.

ACKNOWLEDGMENTS

K.S. is grateful for support from the NSF CAREER Award (grant no. 1350829), the DARPA BTO (grant no. HR0011-16-2-0011), and the NIH (grant no. R01-GM124472). A.T.B. is grateful for support from the NSF Graduate Research Fellowship Program (grant no. 1444932). V.P.-Y.M. is supported by the National Cancer Institute Predoctoral to Postdoctoral Fellow Transition Award (grant no. F99CA223074). This project was supported in part by the Robert P. Apkarian Integrated Electron Microscopy Core. We thank Mr. Qiliang Liu and Mr. Qiongyi Shang for performing AFM imaging. We thank Dr. T. Lian (Emory University, Atlanta, GA) for providing AFM access.

REFERENCES

(1) Yu, H.; Siewny, M. G.; Edwards, D. T.; Sanders, A. W.; Perkins, T. T. *Science* **2017**, *355*, 945−950.
(2) Rief, M.; Gautel, M.; Oesterhelt, F.; Fernandez, J. M.; Gaub, H. E. *Science* **1997**, *276*, 1109−12.
(3) Rico, F.; Gonzalez, L.; Casuso, I.; Puig-Vidal, M.; Scheuring, S. *Science* **2013**, *342*, 741−3.
(4) Hugel, T.; Holland, N. B.; Cattani, A.; Moroder, L.; Seitz, M.; Gaub, H. E. *Science* **2002**, *296*, 1103−6.
(5) Neupane, K.; Foster, D. A.; Dee, D. R.; Yu, H.; Wang, F.; Woodside, M. T. *Science* **2016**, *352*, 239−42.
(6) van Mameren, J.; Gross, P.; Farge, G.; Hooijman, P.; Modesti, M.; Falkenberg, M.; Wuite, G. J.; Peterman, E. J. *Proc. Natl. Acad. Sci. U. S. A.* **2009**, *106*, 18231−6.
(7) Ma, J.; Bai, L.; Wang, M. D. *Science* **2013**, *340*, 1580−3.
(8) Lipfert, J.; Hao, X.; Dekker, N. H. *Biophys. J.* **2009**, *96*, 5040−9.
(9) Neuman, K. C.; Nagy, A. *Nat. Methods* **2008**, *5*, 491−505.
(10) Dufrene, Y. F.; Evans, E.; Engel, A.; Helenius, J.; Gaub, H. E.; Muller, D. J. *Nat. Methods* **2011**, *8*, 123−7.
(11) Halvorsen, K.; Wong, W. P. *Biophys. J.* **2010**, *98*, L53−5.
(12) Yang, D.; Ward, A.; Halvorsen, K.; Wong, W. P. *Nat. Commun.* **2016**, *7*, 11026.
(13) Nickels, P. C.; Wunsch, B.; Holzmeister, P.; Bae, W.; Kneer, L. M.; Grohmann, D.; Tinnefeld, P.; Liedl, T. *Science* **2016**, *354*, 305−307.
(14) Huang, J.; Zarnitsyna, V. I.; Liu, B.; Edwards, L. J.; Jiang, N.; Evavold, B. D.; Zhu, C. *Nature* **2010**, *464*, 932−6.
(15) Liu, B.; Chen, W.; Evavold, B. D.; Zhu, C. *Cell* **2014**, *157*, 357−68.
(16) Liu, Z.; Liu, Y.; Chang, Y.; Seyf, H. R.; Henry, A.; Mattheyses, A. L.; Yehl, K.; Zhang, Y.; Huang, Z.; Salaita, K. *Nat. Methods* **2016**, *13*, 143−6.
(17) Huang, X.; Neretina, S.; El-Sayed, M. A. *Adv. Mater.* **2009**, *21*, 4880−910.
(18) Liu, Y.; Galior, K.; Ma, V. P.; Salaita, K. *Acc Chem Res* **2017**, *50*, 2915−2924.
(19) Woodside, M. T.; Behnke-Parks, W. M.; Larizadeh, K.; Travers, K.; Herschlag, D.; Block, S. M. *Proc. Natl. Acad. Sci. U. S. A.* **2006**, *103*, 6190−5.
(20) Zhang, Y.; Ge, C.; Zhu, C.; Salaita, K. *Nat. Commun.* **2014**, *5*, 5167.
(21) Zhang, Y.; Qiu, Y.; Blanchard, A. T.; Chang, Y.; Brockman, J. M.; Ma, V. P.; Lam, W. A.; Salaita, K. *Proc. Natl. Acad. Sci. U.S.A* **2018**, *115*, 325−330.
(22) Liu, Y.; Blanchfield, L.; Ma, V. P.; Andargachew, R.; Galior, K.; Liu, Z.; Evavold, B.; Salaita, K. *Proc. Natl. Acad. Sci. U. S. A.* **2016**, *113*, 5610−5.
(23) Ma, V. P.-Y.; Liu, Y.; Blanchfield, L.; Su, H.; Evavold, B. D.; Salaita, K. *Nano Letters* **2016**, *16*, 4552−4559.
(24) Bosaeus, N.; El-Sagheer, A. H.; Brown, T.; Smith, S. B.; Akerman, B.; Bustamante, C.; Norden, B. *Proc. Natl. Acad. Sci. U. S. A.* **2012**, *109*, 15179−84.
(25) Bustamante, C.; Bryant, Z.; Smith, S. B. *Nature* **2003**, *421*, 423−7.
(26) Cluzel, P.; Lebrun, A.; Heller, C.; Lavery, R.; Viovy, J. L.; Chatenay, D.; Caron, F. *Science* **1996**, *271*, 792−794.

DOI: 10.1021/acs.nanolett.8b00459
Nano Lett. 2018, 18, 2630−2636

(27) Wang, X.; Ha, T. *Science* **2013**, *340*, 991−4.
(28) Hatch, K.; Danilowicz, C.; Coljee, V.; Prentiss, M. *Phys. Rev. E Stat Nonlin Soft Matter Phys.* **2008**, *78*, 011920.
(29) Seo, D.; Southard, K. M.; Kim, J. W.; Lee, H. J.; Farlow, J.; Lee, J. U.; Litt, D. B.; Haas, T.; Alivisatos, A. P.; Cheon, J.; Gartner, Z. J.; Jun, Y. W. *Cell* **2016**, *165*, 1507−18.
(30) Ma, V. P.; Liu, Y.; Yehl, K.; Galior, K.; Zhang, Y.; Salaita, K. *Angew Chem Int Ed Engl* **2016**, *55*, 5488−92.
(31) Chang, W. S.; Ha, J. W.; Slaughter, L. S.; Link, S. *Proc. Natl. Acad. Sci. U. S. A.* **2010**, *107*, 2781−6.
(32) Ma, H.; Bendix, P. M.; Oddershede, L. B. *Nano Lett.* **2012**, *12*, 3954−60.
(33) Wang, J.; Gan, D.; Lyon, L. A.; El-Sayed, M. A. *J. Am. Chem. Soc.* **2001**, *123*, 11284−9.
(34) Reese, C. E.; Mikhonin, A. V.; Kamenjicki, M.; Tikhonov, A.; Asher, S. A. *J. Am. Chem. Soc.* **2004**, *126*, 1493−6.

DOI: 10.1021/acs.nanolett.8b00459
Nano Lett. 2018, 18, 2630−2636